

Article

Hydrogenation of Flax Shives in Ethanol over a Ni/C Catalyst

Angelina V. Miroshnikova^{1,2}, Aleksandr S. Kazachenko^{1,2,3,*} , Valery E. Tarabanko^{1,*} , Valentin V. Sychev^{1,2} ,
Andrey M. Skripnikov^{1,2}, Yuri L. Mikhlin¹ , Yuriy Kosivtsov⁴, Anna I. Chudina¹ and Oxana P. Taran^{1,2}

¹ Institute of Chemistry and Chemical Technology, Krasnoyarsk Science Center, Siberian Branch, Russian Academy of Sciences, Akademgorodok 50, bld. 24, Krasnoyarsk 660036, Russia

² Department of Non-Ferrous Metals and Materials Science, Siberian Federal University, pr. Svobodny 79, Krasnoyarsk 660041, Russia

³ Department of Biological Chemistry with Courses of Pharmaceutical, Medical and Toxicological Chemistry, Krasnoyarsk State Medical University, st. Partizan Zheleznyak, bld. 1, Krasnoyarsk 660022, Russia

⁴ Department of Biotechnology, Chemistry and Standardization, Tver State Technical University, 22 nab. A. Nikitina, Tver 170026, Russia

* Correspondence: leo_lion_leo@mail.ru (A.S.K.); veta@icct.ru (V.E.T.)

Abstract: Hydrogenation of flax shives in ethanol over bifunctional Ni/C catalysts at 225 °C has been studied. It has been shown that the 10% Ni/C catalyst enhances the yield of monomeric products from 1.1 to 9.7 wt %, decreases the solid product content from 45 to 35 wt %, and increases the degree of delignification to 91%. The main monomeric compounds obtained during hydrogenation are propyl guaiacol and propenyl guaiacol. It has been established that an increase in the mass transfer intensity via increasing the stirring rate or decreasing the catalyst grain size leads to an increase in the total yield of monomeric compounds and the propanol guaiacol yield. Alkaline and acid pretreatment increases the cellulose content in the solid product from 42 to 73 wt %. The proposed sequential scheme of the transformation and formation of monomeric products over the bifunctional nickel catalyst is lignin—coniferyl alcohol—4-propanol guaiacol—4-propenyl guaiacol—4-propyl guaiacol.

Keywords: flax shives; hydrogenation; mass transfer; ethanol; Sibunit; Ni/C catalyst; guaiacyl propanes



Citation: Miroshnikova, A.V.; Kazachenko, A.S.; Tarabanko, V.E.; Sychev, V.V.; Skripnikov, A.M.; Mikhlin, Y.L.; Kosivtsov, Y.; Chudina, A.I.; Taran, O.P. Hydrogenation of Flax Shives in Ethanol over a Ni/C Catalyst. *Catalysts* **2022**, *12*, 1177. <https://doi.org/10.3390/catal12101177>

Academic Editor: S David Jackson

Received: 8 August 2022

Accepted: 27 September 2022

Published: 5 October 2022

Publisher's Note: MDPI stays neutral with regard to jurisdictional claims in published maps and institutional affiliations.



Copyright: © 2022 by the authors. Licensee MDPI, Basel, Switzerland. This article is an open access article distributed under the terms and conditions of the Creative Commons Attribution (CC BY) license (<https://creativecommons.org/licenses/by/4.0/>).

1. Introduction

Global warming related to carbon dioxide emissions and the depletion of fossil resources requires advanced methods for the use of renewable plant-based raw materials, including a lot of cheap agricultural waste (1.5 billion tons per year) [1–5]. Flax shives, a lignified part of the stem, are the main flax fiber production waste (up to 70 wt %). They consist of lignin (~25%), cellulose (~50%), and hemicelluloses (~20%) [1,6].

To process all components of lignocellulosic biomass, it is subjected to catalytic fractionation by methods based on selective oxidation (with hydrogen peroxide [7] or oxygen [8]) or reduction (with hydrogen and hydrogen donor agents [9–11]). The hydrogen donor agents used are aliphatic alcohols (methanol, ethanol, or isopropanol) [11–13] and formic acids [14,15]. The reductive catalytic fractionation of lignocellulosic biomass ensures depolymerization of lignin with the formation of monomer compounds whilst maintaining the main part of cellulose [16,17].

The reductive catalytic fractionation occurs over heterogeneous bifunctional catalysts [18–20]. The possibility of using bifunctional catalysts containing Ru and Ni nanoparticles on a Sibunit mesoporous carbon support modified with oxygen-containing groups for the catalytic hydrogenolysis of organosolv birch lignin in ethanol was shown in [21,22]. Such catalysts increase the yield of liquid product and decrease gaseous and coke yields. Ru is the most efficient catalyst for the aqueous-phase hydrogenation of biosourced compounds [23]. Moreover, nickel is one of the most popular metals due to its high efficiency in the hydrogenolysis of the C–O bond and high selectivity towards aromatic compounds [24].

Moreover, it was shown [25] that Ru/C and Ni/C catalysts provide the same monomer yields (~25 wt %) from corn stover lignin.

A study of the effect of a nickel catalyst loading on the yield of main birch wood fractionation products [26] showed that the maximum monomer yields (~30 wt %) correspond to a catalyst loading of 10% of the wood mass (11 wt % of Ni per carbon support).

As we showed previously [27], the acid pretreatment of birch wood affects the yield and composition of the products of its catalytic hydrogenation more strongly than the alkaline pretreatment; however, the maximum total content of methoxyphenols (24.46 wt %) is observed in liquid products of catalytic hydrogenation of birch wood subjected to the alkaline treatment.

In this work, we examine the effect of the content of nickel deposited onto an oxidized graphite-like Sibunit carbon support and the impact of mass transfer intensity and pretreatments of flax shives on the process of its fractionation.

2. Results and Discussion

2.1. Texture Characteristics of the Catalysts

The texture characteristics obtained using the low-temperature nitrogen adsorption method showed that, in the series S450—5NiS450—10NiS450—20NiS450 (Table 1), the precipitation of nickel leads, due to the partial blocking of the support pores, to a monotonic decrease in the specific surface area from 380 to 276 m²/g; in the pore volume, from 0.53 to 0.42 cm³/g; and in the average pore size from 5.66 to 5.42 nm. Obtained isotherm profiles correspond to type IV nitrogen adsorption-desorption isotherms for the BET surface area analysis inherent to mesoporous materials (Figure 1).

Table 1. Characteristics of the carbon support and nickel catalysts based on it.

No.	Support/ Catalyst	Code	Ni Particle Size, nm ⁷	Ni Particle Size, nm ⁸			pH _{PZC} ¹	Texture Characteristics ²		
				d _{min}	<d _l >	d _{max}		S _{BET} , m ² /g	V _{pore} , cm ³ /g	<d _{pore} >, nm
1	Sib-4-ox450 ³	S450	-	-	-	-	5.33	380	0.53	5.66
2	5%Ni/Sib-4-ox-450 ³	5NiS450	20.17	45	127	324	8.15	350	0.52	5.64
3	10%Ni/Sib-4-ox-450 ³	10NiS450	21.39	63	152	351	8.70	315	0.51	5.61
4	20%Ni/Sib-4-ox-450 ³	20NiS450	28.25	77	172	400	9.86	276	0.42	5.42
5	10%Ni/Sib-4-ox-450g ⁴	10NiS450g	-	-	-	-	8.70	315	0.51	5.61
6	10%Ni/Sib-4-ox-450-100 ⁵	10NiS450-100	-	-	-	-	8.70	315	0.51	5.61
7	10%Ni/Sib-4-ox-450-250 ⁶	10NiS450-250	-	-	-	-	8.70	315	0.51	5.61

¹ pH_{PZC} is the pH of the point of zero charge; ² The texture characteristics were obtained by processing the low-temperature nitrogen adsorption data. S_{BET} is the specific surface according to the BET model (m²/g), V_{pore} is the total pore volume (cm³/g), and <d_{pore}> is the average pore size (nm); ³ The fraction of 56–94 μm; ⁴ The fraction of 1.0–1.6 mm; ⁵ The fraction of 100–250 μm; ⁶ The fraction of 250–500 μm; ⁷ The particle size is determined using the Scherrer equation on the basis of the Ni(200) reflection; ⁸ Statistical processing of the SEM images (magnification of up to ×20.0 k); d_{min} and d_{max} are the minimum and maximum particle diameters and <d_l> = Σd_i/N is the average particle size.

pH_{PZC} value increases (and, hence, the catalysts' acidity decreases) with the increasing Ni content in the catalysts' series S450 support, 5NiS450, 10NiS450, and 20NiS450 from pH_{PZC} 5.33 up to 9.86 (Table 1). This dependence may be connected with bonding acid sites by Ni ions.

The morphology of the catalysts was studied by scanning electron microscopy (magnification of up to ×20.0 k). The images were subjected to statistical processing and the Ni particle distribution over the surface at different Ni contents in the catalyst was tested. The catalysts with a lower Ni content have a more uniform particle size distribution. As the nickel content increases, the minimum (45–63–77 nm), average (127–152–172 nm), and maximum (324–351–400) particle sizes increase in the series 5NiS450, 10NiS450, and 20NiS450 (Table 1, Figure 2).

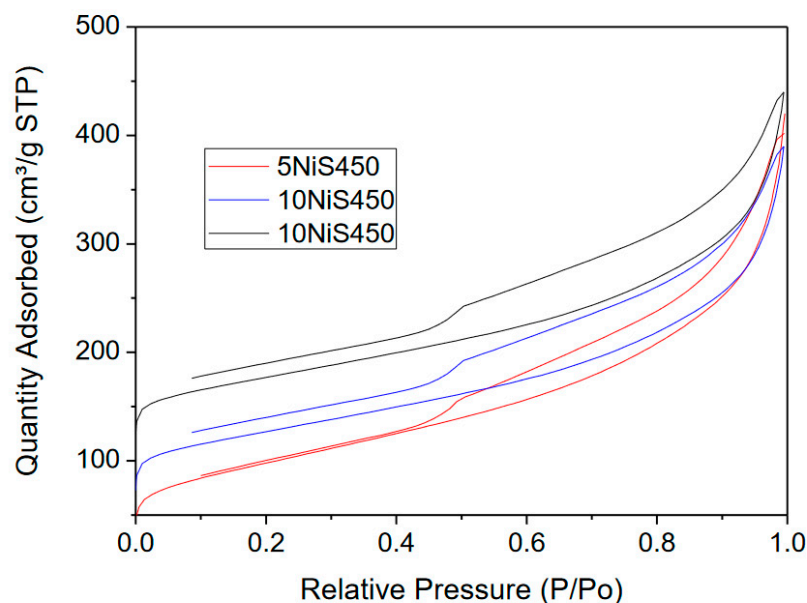


Figure 1. Nitrogen adsorption-desorption isotherms of 5NiS450, 10NiS450, and 20NiS450.

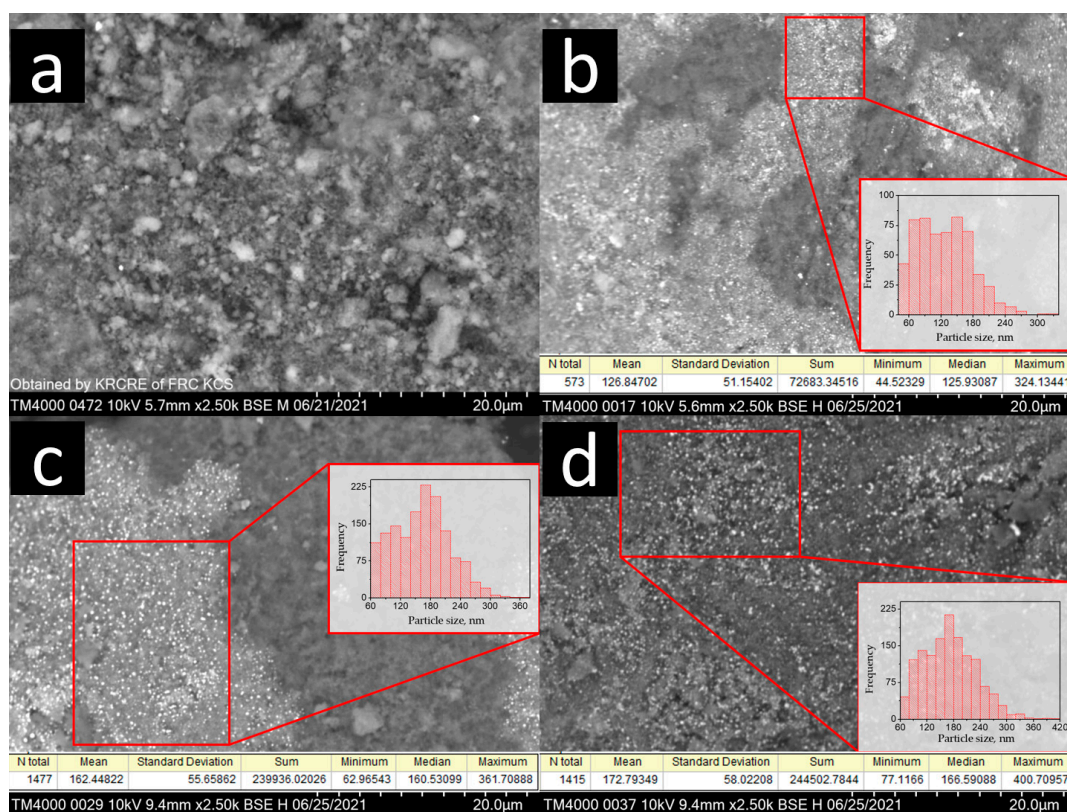


Figure 2. Microphotographs of (a) the S450, (b) 5NiS450, (c) 10NiS450, and (d) 20NiS450 catalysts.

The 10NiS450 catalyst was examined by transmission electron microscopy and the images obtained were statistically processed. Despite the presence of relatively large (100–400 nm) nickel-containing agglomerates on the surface, the distribution of which was studied by scanning electron microscopy, the main fraction of nickel on the surface is formed by nickel particles smaller than 50 nm in size, so the average particle size is 26 nm (Figure 3).

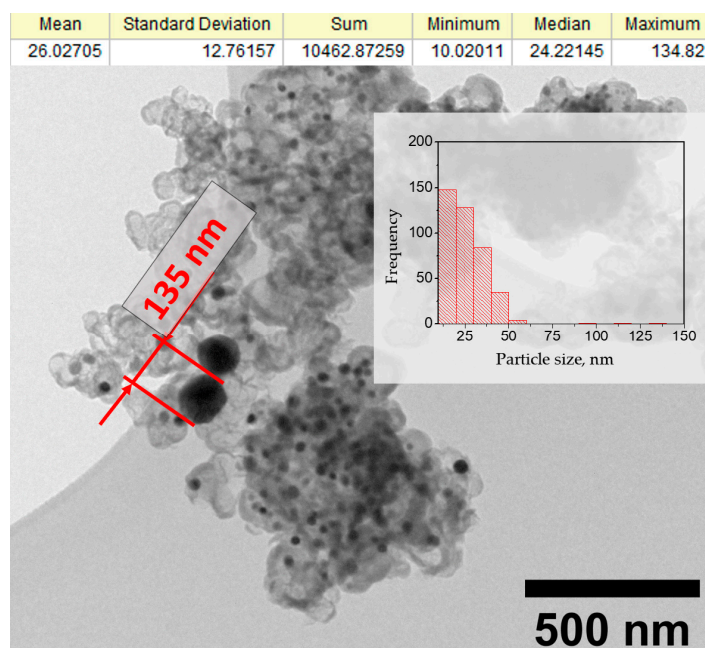


Figure 3. TEM image of the 10NiS450 catalyst.

X-ray diffraction analysis of the catalysts allowed us to establish the electronic state of nickel and size distribution of its particles, which are inaccessible by scanning electron microscopy. The X-ray diffraction patterns contain the (111), (200), and (220) reflections characteristic of metal nickel at 2θ angles of 44, 52, and 76, respectively (Figure 4). The nickel particle size was calculated using the Scherrer equation on the basis of the (200) reflection. The nickel particle size increases with the nickel content in the series 5NiS450–10NiS450–20NiS450 and amounts to 20.2–21.4–28.3 nm, respectively (Table 2).

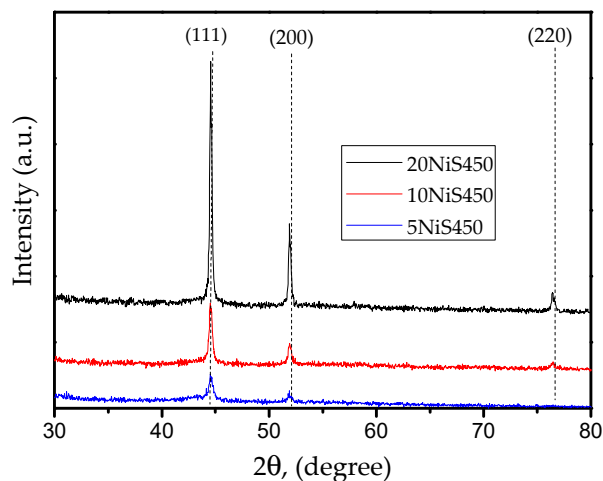


Figure 4. X-ray diffraction patterns of the nickel catalysts based on the Sibunit carbon material with nickel contents of 5, 10, and 20%.

Table 2. XPS elemental composition of the catalyst surface.

Catalyst	C		O		Ni	
	at %	wt %	at %	wt %	at %	wt %
20NiS450	95.63	89.9	2.97	3.7	1.4	6.4
10NiS450	97.37	94.6	2.03	2.6	0.58	2.8
5NiS450	98.08	96.1	1.52	2.0	0.41	2.0

The chemical state of the catalyst surface was thoroughly investigated by X-ray photoelectron spectroscopy (XPS). The results obtained are given in Table 2. The 5NiS450, 10NiS450, and 20NiS450 catalysts are characterized by peaks at 852.9, 854.5, and 855.8 eV, which correspond to the Ni⁰, Ni²⁺, and Ni³⁺ states, respectively (Figures 5 and 6) [28]. In the range of 283–293 eV, the peak characteristic of graphite is the most intense; in addition, the spectrum contains peaks of amorphous carbon, carbonyl, hydroxyl, and ether groups, as well as fragments of carboxyl groups (Figure 6) [29]. No signals characteristic of chlorine were found in the spectra, which shows the effective removal of the Cl[−] counterion under the catalyst reduction conditions.

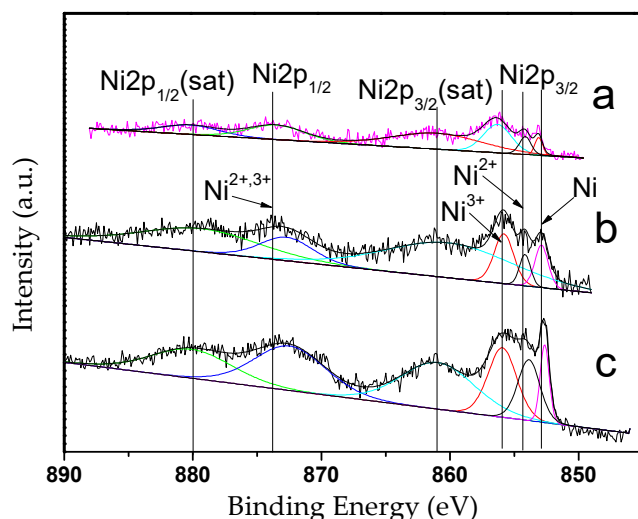


Figure 5. Ni2p XPS spectra of catalysts (a) 5NiS450, (b) 10NiS450, and (c) 20NiS450.

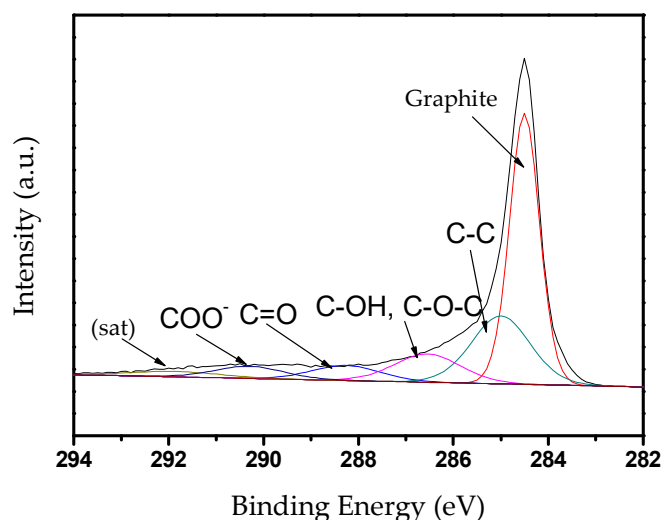


Figure 6. C1s XPS spectrum of the 10% Ni catalyst based on an S450 oxidized carbon support.

2.2. Reductive Catalytic Fractionation of Flax Shives

Tables 3 and 4 show the results of the reductive catalytic fractionation of flax shives over the Ni/C catalyst with different nickel contents and, for comparison, similar data on a ruthenium catalyst [30]. Using the most active nickel catalyst (10NiS450) increases the degree of delignification and monomeric product yield by a factor of 1.5 and 9, respectively. This catalyst inferior the ruthenium one in terms of monomer yield by 1.3 times, but exceeds it on the degree of delignification. The cellulose yield drops under the action of the catalysts from 55 to 42–52% of the cellulose content in the feedstock, except for the 5NiS450 catalyst, which provides the cellulose yield maximum (65%).

Table 3. Effect of the metal content in a catalyst on the fractionation product yield of flax shives (225 °C, 3 h).

Conditions	Yields, wt %		
	Liquid	Solid	Monomers
No catalyst	36.4	45.4	1.14
5NiS450	29.0	41.6	5.28
10NiS450	32.0	34.9	9.67
20NiS450	30.4	41.0	8.75
3Ru/S450 [30]	42.5	33.0	12.2

Table 4. Effect of the metal content in the catalyst on the composition of solid products from the fractionation of flax shives (225 °C, 3 h).

Conditions	Content			Cellulose Yield, % *	Delignification, %
	Lignin	Cellulose	Hemicelluloses		
No catalyst	27.3	68.5	4.2	55.4	63.3
5NiS450	16.7	79.3	4.0	64.7	85.1
10NiS450	11.5	86.4	2.1	42.2	90.6
20NiS450	12.7	83.6	3.7	51.4	87.0
3Ru S450 [30]	15.5	79.5	5.8	51.8	83.2

* Weight ratio between cellulose in the solid product and the initial shives sample.

The data on the effect of the nickel catalysts on the liquid product yields look unexpected: the latter reproducibly decrease from 36 to 29–32%. This dependence can be explained by the next assumption: some of the primary products of catalytic delignification are condensed into insoluble in ethanol substances, which are not identified as lignin or cellulose, i.e., dissolved in the sulfuric acid solution. As for the more active ruthenium catalysts, such condensation is not observed.

The efficiency of the ruthenium catalysts is higher than that of the nickel ones by a third in the liquid product yield and by a quarter in the yields of monomeric products and cellulose. This is probably due to the fact that two parallel destruction and condensation reactions occur in this process, and on a nickel catalyst it is not possible to accelerate the destruction as effectively to suppress the condensation reaction as on a ruthenium catalyst (Table 5).

Table 5. Effect of the metal loading on the yields of main monomers (225 °C, 3 h).

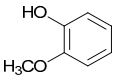
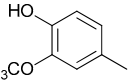
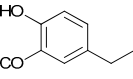
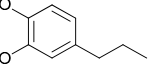
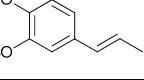
RT *	Substance	Structure	Sample				
			No Catalyst	5NiS450	10NiS450	20 NiS450	3RuS450 [30]
17.71	Guaiacol		0.36	0.47	0.44	0.55	0.55
21.29	Methyl guaiacol		0.01	0.10	0.09	0.06	0.01
23.96	Ethyl guaiacol		0.21	0.29	0.33	0.35	0.88
25.98	Propyl guaiacol		0.08	0.34	2.73	1.33	4.95
26.44	Propenyl guaiacol		0.19	0.36	1.53	2.07	1.17

Table 5. Cont.

RT *	Substance	Structure	Sample				
			No Catalyst	5NiS450	10NiS450	20 NiS450	3RuS450 [30]
28.58	Ethyl syringol		0.04	0.09	0.12	0.10	0.24
30.49	Propyl syringol		0.03	0.47	0.88	0.47	1.26
32.47	Propanol guaiacol		0.08	0.23	1.58	1.59	1.09
34.51	Propenyl syringol		0.14	0.19	0.12	0.08	0.06
	Main methoxyphenols		1.14	2.54	7.82	6.60	10.21
	Other monomers		0.52	2.74	1.85	2.15	2.00
	Total monomer yield, wt %		1.66	5.28	9.67	8.75	12.21

* retention time.

Taking into account the structure of lignin, methoxylated phenols can be the most interesting and promising products of its processing [31]. The main monomeric derivatives are 4-propyl, propenyl, and propanol substituted guaiacols. Hydrogenation of beech lignocellulosic biomass over nickel catalysts yields 4-propanol syringol and 4-propanol guaiacol as the main product [32]. According to the data given in Table 5, during hydrogenation of flax shives, the yield of 4-propanol guaiacol increases from 0.23 to 1.58 wt % with an increase in the Ni content in the catalyst from 5 to 10%. At the same time, the yield of the main product—4-propyl guaiacol increases from 0.34 to its maximum value of 2.73 wt %. As the Ni content further increases to 20%, the 4-propyl guaiacol yield drops, while the 4-propanol guaiacol yield remains unchanged. Ni loading is not the factor completely defining the catalysts' activity. However, the ratio Ni⁰/NiO_x is the amount of surface metallic nickel in relation to its oxides (Table 6) and sheds a light on catalyst performance related to the amount of specific phase of Ni present. A higher Ni⁰/NiO_x ratio provides a higher total product yield and shifts the selectivity in monomer formation toward propyl substituted monophenols (the products of deeper hydrogenation) (Tables 5 and 6; Figure 7).

Table 6. Influence of catalyst surface nickel electronic state on the product yield.

Catalyst	Fraction of a Metal in the Oxidation Degree, % *			Ni ⁰ /NiO _x	4-propylguaiacol Yield, wt %	4-propylsyringol Yield, wt %	Total Products Yield, wt %
	Ni ³⁺	Ni ²⁺	Ni ⁰				
5NiS450	69.8	18.4	11.8	0.134	0.34	0.47	5.28
10NiS450	51.5	18.2	30.3	0.434	2.73	0.88	9.67
20NiS450	49.2	33.4	17.4	0.210	1.33	0.47	8.75

* The data were obtained by deconvolution of the XPS spectra of Ni 2p_{3/2} into individual states.

2.3. Effect of Pretreatment of Flax Shives on Their Subsequent Hydrogenation

The flax shives were subjected to acid and alkaline pretreatment in order to remove xylan and activate lignin [33]. Xylan is used in many areas of industry [34]. The most common type of hemicelluloses in hardwoods and herbaceous plants is xylan [35]. Preliminary removal of xylan followed by hydrogenation of biomass is a new approach to the complex processing of plant materials.

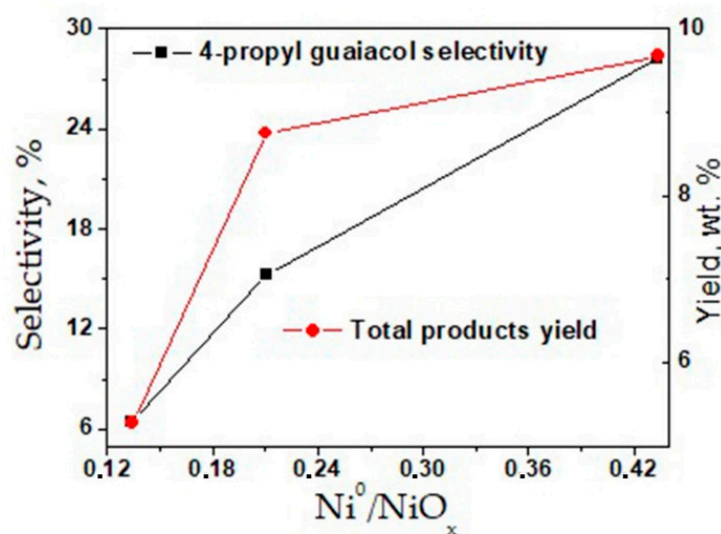


Figure 7. The influence of Ni⁰/NiO_x ratio on selectivity to 4-propylguaiacol and total product yield.

Lignin creates the phenyl glycosidic bonds with biomass polysaccharides forming the so-called lignocarbohydrate complex [36]. The chemical bonds between lignin and hemicelluloses significantly affect the reactivity of biomass [37]. Acid and alkaline pretreatments may disrupt the native structure of the lignocarbohydrate complex and change its reactivity [33]. The acid pretreatment selectively hydrolyzes hemicelluloses in lignocellulosic biomass [38] and can significantly change the lignin structure [39]. The alkaline treatment of biomass ensures its efficient delignification under milder conditions [40].

The obtained results show that both acid and alkaline prehydrolysis of flax shives before their hydrogenation slightly (within 91–93%) changes the degree of delignification. Both types of prehydrolysis increase the yield of cellulose (from 42 to 60–73%) and solids in general (from 35 to 44–51%) (see Tables 7 and 8), and decrease the content of lignin (from 12 to 7–9%) and hemicellulose (from 2 to 1–2%).

Table 7. Effect of pretreatments of flax shives on the yield of the main products in the followed fractionation process (225°C, 10NiS450).

Treatment Conditions	Yields, wt %			Cellulose Yield, wt % of Initial	Delignification, %
	Liquid	Solid	Monomers		
Initial	31.99	34.92	9.67	42.2	90.6
HCl	29.25	43.73	6.49	60.2	92.6
NaOH	22.88	50.97	9.50	72.8	89.9

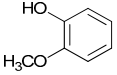
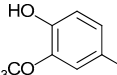
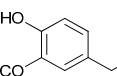
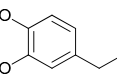
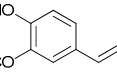
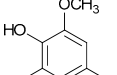
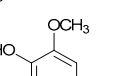
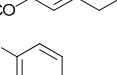
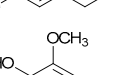
The alkaline and acid pretreatment of the shives reduces the yields of the main monomeric products, propyl-, propenyl-, and propanol guaiacols (Table 8). The alkaline pretreatment of raw materials is of the greatest interest for increasing the efficiency of the catalytic fractionation of flax shives, since it enables the cellulose yield to increase by a factor of 1.7 for the invariable yields of monomeric products (Tables 7 and 8). The xylan yield was 12.8% of the air-dry initial flax shives.

2.4. Effect of the Stirring Rate and Catalyst Grain Size on the Hydrogenation Process

Mass transfer intensity is one of the important factors affecting the hydrogenation process, but its influence on the processing of lignins has not been studied yet. Table 9 gives the data on the effect of the stirring rate and catalyst grain size on the composition of the solid products of the hydrogenation of flax shives. The effect of these parameters on the behavior of lignin looks quite predictable: an increase in the stirring rate and a decrease in the catalyst grain size enhance the degree of delignification and, consequently, reduce the

lignin content in the solid residue. Similarly, an increase in the intensity of mass transfer reduces the content of hemicelluloses in the solid residue.

Table 8. Effect of pretreatments of flax shives on the yield of monomeric compounds in the followed fractionation process (225 °C, 3 h, 10NiS450).

RT *	Substance	Structure	Sample Pretreatment		
			Initial	Acidic	Alkaline
17.71	Guaiacol		0.44	0.30	0.95
21.29	Methyl guaiacol		0.09	0.08	0.16
23.96	Ethyl guaiacol		0.33	0.21	0.46
25.98	Propyl guaiacol		2.73	1.44	1.92
26.44	Propenyl guaiacol		1.53	0.59	1.06
28.58	Ethyl syringol		0.12	0.06	0.12
30.49	Propyl syringol		0.88	0.46	1.14
32.47	Propanol guaiacol		1.58	0.43	1.48
34.51	Propenyl syringol		0.12	0.30	0.12
	Total alkyphenol yield, wt %		7.82	3.87	7.41
	Other monomers		1.85	2.72	2.09
	Total monomer yield, wt %		9.67	6.59	9.50

* RT is the retention time.

Table 9. Effect of the stirring rate and catalyst grain size on the solid product yield from the fractionation of flax shives (10NiS450, 225 °C).

Fraction, μm	Stirring, rpm	Content, wt %			Cellulose Yield, wt %	Delignification, %
		Lignin	Cellulose	Hemicelluloses		
54–96	1000	11.5	86.4	2.1	42.2	90.6
100–250		13.7	84.2	2.1	64.9	85.5
250–500		15.2	82.6	2.2	65.8	82.3
1–2 mm	125	17.3	80.4	2.3	66.7	79.0
		25.2	70.9	3.9	91.6	70.1
54–96	250	19.0	77.6	3.4	90.9	77.4
	500	12.1	85.1	2.8	84.6	86.1
no catalyst	1000	27.3	68.5	4.2	55.4	63.3

An increase in the stirring rate, as well as a decrease in the catalyst grain size during the process, leads to the monotonic growth of the monomeric compound yield from 1.5 to 9.7 wt % (Table 10). The comparison of the effect of the catalyst grain size and the stirring rate on the process shows that, qualitatively, both factors similarly affect the conversion of

lignin and hemicelluloses, as well as the yield of liquid products. This analogy indicates that both the catalyst grain size and stirring rate influence the rate of the process occurring on the outer surface of a catalyst grain under the conditions of external diffusion limitation. A decrease in the catalyst grain size leads to an increase in the outer surface area and an increase in the intensity of mass transfer enhances the concentration of reagents on the surface. Both effects increase the process rate.

Table 10. Effect of the stirring rate and catalyst grain size on the composition of the products from the fractionation of flax shives (10NiS450, 225 °C).

Fraction, μm	Stirring, rpm	Yields, wt %		
		Liquid	Solid	Monomers
54–96	1000	31.99	34.92	9.67
100–250		27.83	36.55	7.26
250–500		30.96	38.89	6.84
1–2 mm;		29.46	42.96	4.07
	125	14.62	74.36	1.46
54–96	250	17.24	59.26	3.91
	500	24.63	50.46	8.08
No catalyst	1000	38.5	41.0	1.14

The dependence of the cellulose yield on the mass transfer conditions is more complex. Judging by the effect of the catalyst grain size at the maximum stirring rate, the catalyst drives two processes of cellulose conversion; it stabilizes cellulose at large grain sizes (0.1–2 mm) and destructs it at the minimum grain size, i.e., at the maximum catalyst activity. A decrease in the stirring rate by a factor of 2–8 on the most active catalyst form causes an increase in the cellulose yield by a factor of two or more, up to 92%, i.e., almost to the initial content in the shives. Thus, the best compromise on the cellulose yield and degree of delignification (85 and 86%, respectively) is observed at the minimum grain size (54–96 μm) and mild stirring rate (500 min^{-1}). This compromise may be associated with different rates of lignin and cellulose destruction under the hydrogenation conditions.

The unexpected inhibition of the liquid product formation by the catalyst was discussed above (see Table 3 and the discussion). A similar effect was observed for the mass transfer influence on the liquid product yield. At any stirring intensity, the yields of liquid products in the catalytic process increase with the mass transfer rate (from 15 to 25 wt %), but do not attain the yield value in the non-catalytic process (39 wt %). This means that the primary liquid delignification products formed without a catalyst are partially condensed into insoluble ones under the action of the catalyst and this process slows down with an increase in the mass transfer intensity. The simplest explanation for this fact is that the process efficiency is limited by the rate of removal of final and intermediate products from catalyst pores, which is comparable to the rate of catalytic condensation of soluble products into the products determined as solids. A similar situation is observed for the yield of the solid product of catalytic fractionation: only at the highest stirring rate, the yield of an insoluble solid substrate appears lower than in the non-catalytic process. In this case, a change in the catalyst grain size does not significantly affect the yields of liquid and solid products (Table 10).

Correspondingly, the stirring rate greatly affects the composition of monomeric products. Trace amounts of coniferyl alcohol were found only at low (125–500 min^{-1}) stirring rates. The yield of the final product, 4-propyl guaiacol, increases monotonically with an increase in the stirring rate; a similar increase in its yield with a decrease in the catalyst grain size is observed, but less pronounced. The dependences of the 4-propenyl guaiacol yield on the mass transfer intensity are similar, except for the maximum point (1000 min^{-1} , 56–94 μm). 4-propanolguaiacol was only detected in this experiment at the maximum mass transfer intensity (Figure 8). A similar change in the main products from propanol-substituted methoxyphenols to 4-propylguaiacol and 4-propylsyringol is observed while

adding molecular hydrogen to a process of fractionation of birch wood over a Ni-based catalyst in methanol [24,41].

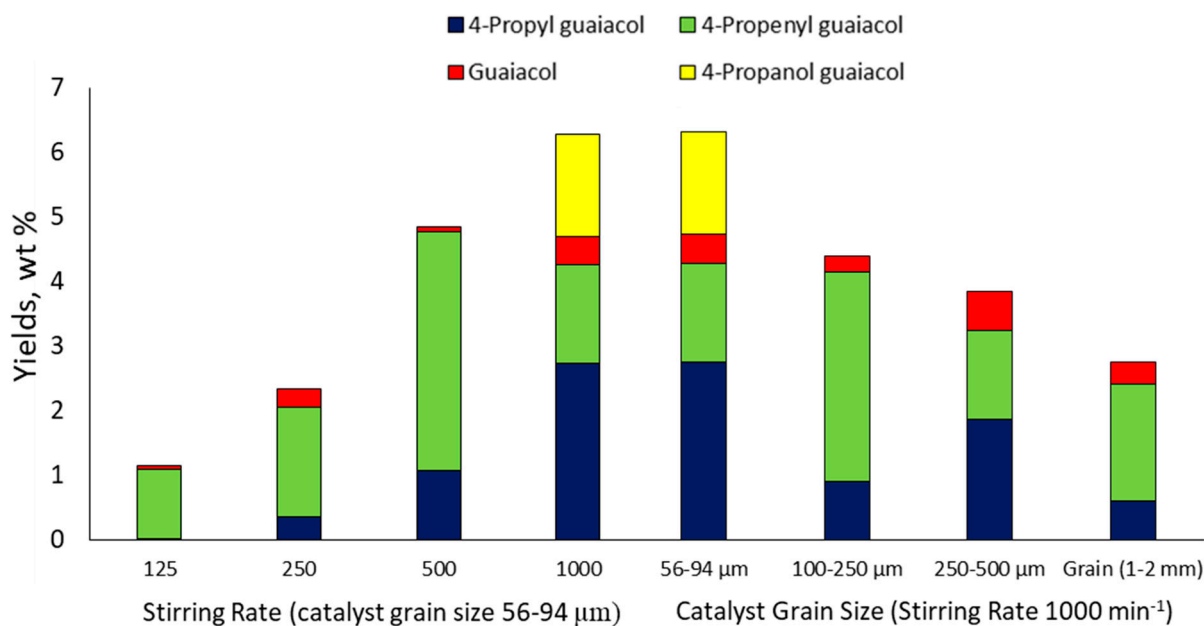


Figure 8. Effect of the stirring rate and catalyst particle size on the yield of main monomeric compounds.

The obtained results confirm the earlier suggested sequence of the main stages of the process occurring over a nickel catalyst [42] (Figure 9):

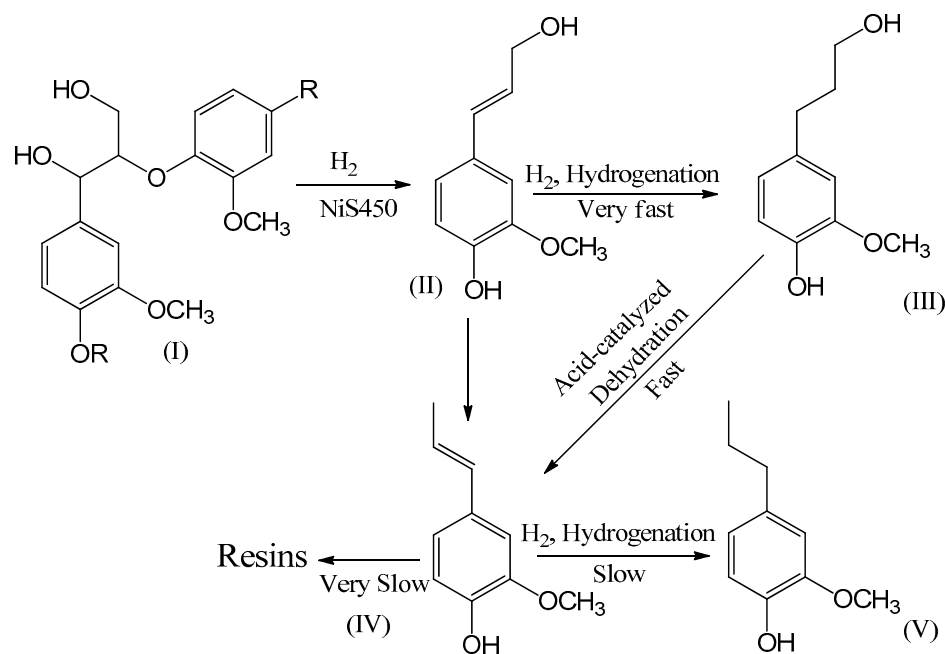


Figure 9. Scheme of depolymerization and conversion of intermediates to 4-propyl guaiacol and 4-propanol guaiacol.

The process begins with the formation of the detected coniferous alcohol (II) found previously in the lignin hydrogenation processes [24,41]. The formation of coniferous lignins by the oxidative condensation of coniferous alcohol is generally recognized and its formation in the hydrogenation processes is quite understandable; it is highly active as compared with the other propyl guaiacol derivatives (III)–(V) and therefore detected

in minor concentrations. Coniferyl alcohol is formed on the catalyst surface; this stage determines the growth of the yield of products (III)–(V) under the action of a catalyst.

4-propanolguaiacol is detected at high mass transfer intensity only. This testifies to the high rates of its transformation on the catalyst surface, and only its intense mass transfer into the bulk of the liquid phase makes it possible to detect 4-propanolguaiacol in the process under study. 4-propenyl guaiacol is one of the main products detected under any mass transfer conditions. The comparison of these two results (Figure 9) points to the acid-catalytic dehydration of 4-propanolguaiacol (III) to 4-propenylguaiacol (IV) at the acid sites of the catalyst surface as the main route of transformation (III). The resulting 4-propenyl guaiacol (IV) is further hydrogenated to 4-propyl guaiacol (V) or resinified.

In the framework of the scheme shown in Figure 9, the stages of hydrogenolysis of C–O bonds of coniferyl alcohol (II) and 4-propanolguaiacol (III) are not required to describe the obtained experimental results.

3. Materials and Methods

3.1. Preparing Flax Shive Samples

Flax shives were provided by the Tver State Technical University. Air-dried flax shives were ground in a VR-2 disintegrator (Moscow, Russia) and then the dry fractionation on sieves was performed. In this study, the flax shives fraction size was 0.5–2 mm. The flax shives components (% of the absolutely dry substrate weight) were cellulose (50.6), lignin (30.4), hemicelluloses (17.1), and ash (1.9). Flax shives were dried at 80 °C to a moisture content of lower than 1 wt %.

3.2. Preparing Nickel Catalysts for Hydrogenation of Shives

Carbon samples were prepared from a commercial mesoporous Sibunit-4 (S4) carbon support (Center of New Chemical Technologies, Boreskov Institute of Catalysis, Siberian Branch, Russian Academy of Sciences, Omsk, Russia). The carbon material was prewashed using boiling deionized water to remove possible metal impurities and dried in an argon flow at 150 °C. To obtain a fraction with a carbon particle size of 56–94 µm, the carbon material was crushed in a porcelain mortar and sieved. The oxidized samples were obtained by oxidation of the Sibunit-4 support with moist air. The oxidation was performed in a quartz cell placed in a furnace. The cell filled with the carbon material was preliminarily purged with argon (200 mL/min, 0.5 h); after that, a mixture of 20 vol % O₂ in N₂ was supplied to the cell in the presence of water vapors at a temperature of 450 °C (the saturation at 90 °C, a vapor pressure of 70.1 kPa, a flow of 200 mL/min, 2 h) [43].

The nickel catalysts based on the oxidized Sibunit-4 carbon support were obtained by wetness impregnation with an aqueous solution of nickel (II) chloride hexahydrate (NiCl₂·6H₂O) followed by drying at room temperature for 3 h and 60 °C for 12 h.

The active component was reduced in a quartz reactor in a hydrogen flow (30 mL/min, 450 °C, 2 h); the temperature was increased at a rate of 8 °C/min; after cooling to room temperature in the hydrogen atmosphere, the catalyst was passivated with the gas mixture containing 1% of O₂ in N₂ (a flow of 200 mL/min, 0.5 h) [43,44].

3.3. Physicochemical Study of the Catalysts

The texture characteristics of the samples were determined from the N₂ adsorption isotherms at 77 K with a Micromeritics ASAP-2020 Plus instrument (Norcross, GA, USA).

X-ray powder diffraction data were obtained on an X'Pert PRO diffractometer with a PIXcel (PANalytical, Almelo, Netherlands) detector (CuK α radiation) equipped with a graphite monochromator. The sample was ground in an agate mortar and prepared by powdering. The analysis was carried out at room temperature in the 2 θ small-angle range from 5 to 80° with a step of 0.026° ($\Delta t = 50$ s).

Photoelectron spectra were recorded on a SPECS spectrometer with a PHOIBOS MCD9 hemispherical energy analyzer under excitation by the monochromatic AlK α radiation at an electron collection angle of 90°. The element contents were determined from the survey

spectra. During the CasaXPS software processing, the Shirley nonlinear background was subtracted and a Gaussian/Lorentzian peak shape was used.

The acidity of the catalysts was estimated from the point of zero charge (PZC) using the Sorenson–de Bruijn method [45]. An amount of 10 mL of distilled water was placed in a potentiometric cell. Then, the investigated sample was added successively in small (0.01 g) portions under continuous stirring with a magnetic stirrer in time intervals of 5–10 min until the constant potential of a glass electrode [45].

The surface morphology was studied on a Hitachi TM4000 Plus scanning electron microscope (Hitachi, Tokyo, Japan) with an attachment for the energy dispersive microanalysis for measuring linear sizes of microrelief elements and the qualitative and quantitative electron probe X-ray microanalysis of the sample composition. Information about the surface was obtained by irradiating the sample with a narrowly focused electron beam. The fine structure of the sample surface was observed by magnifying and displaying the back-scattered and secondary electron data.

High-resolution electron microphotographs of the Ni/C catalysts were obtained on a Hitachi HT7700 transmission electron microscope (Japan, 2014) at an accelerating voltage of 110 kV and a resolution of 2 Å. The microphotographs were statistically processed (500–800 particles) and particle size distribution histograms were built. The elemental analysis of the synthesized composites was carried out on a PANalytical AxiosAdvanced X-ray fluorescence spectrometer. For the analysis, the test material was pressed with boric acid H_3BO_3 as a binder into a tablet 32 mm in diameter.

3.4. Prehydrolysis of Flax Shives

Acid hydrolysis of hemicelluloses was carried out via the treatment of 23% of the shives with hydrochloric acid at room temperature for 1 h [46].

3.4.1. Fat and Wax Removal

An amount of 40 g of air-dried flax shives was treated with 1200 mL of aqueous ethanol (1:1, v:v) for 1 h under the reflux conditions. The sawdust was washed with water and dried to an air-dry state at 55 °C; for one day. The air-dried residue of the shives after the water-alcohol treatment was 35.8 g.

3.4.2. Isolation of Xylan

The flax shives residue (35.8 g) after the water-alcohol extraction was treated with 4% chemically pure sodium hydroxide solution under continuous stirring (a liquor ratio of 1:40 g/mL) at room temperature for 6 h. Then, the solution was filtered on a Buechner funnel and the shives were washed several times on a cotton filter. The obtained solution was neutralized with chemically pure acetic acid until the formation of a flocculent precipitate. After that, the neutralized solution was added with 96% ethyl alcohol in a volume ratio of 1:1. The solution with the precipitate was kept under cooling (+5 °C) for 16–20 h; then, the water-alcohol extract was decanted and the xylan precipitate was added with ethanol again and kept under cooling. Next, the solution was decanted and xylan was centrifuged in an OHAUS Frontier 5816 centrifuge (Parsippany, NJ, USA,) at 8000 rpm for 8 min and subjected to freezing and freeze-drying in an Inei-4 dryer.

The flax shives prehydrolyzed with alkali contained 59.7% of cellulose, 34.7% of lignin, 4.1% of hemicellulose, and 1.5% of ash. The flax shives prehydrolyzed with hydrochloric acid (the weight loss after prehydrolysis was 10%) contained 57.3% of cellulose, 37.4% of lignin, 3.6% of hemicellulose, and 1.7 of ash.

3.5. Hydrogenation of Flax Shives

Flax shives were hydrogenated in a ChemRe SYStem R-201 autoclave (Anyang, Korea) with a volume of 300 mL. The reactor was loaded with 60 mL (1.05 mol) of ethanol, 3.0 g of the substrate, and 0.3 g of the catalyst. The autoclave was sealed and purged with argon to remove air. Then, hydrogen was supplied to an initial pressure of 4 MPa on a manometer.

The reaction occurred at a temperature of 225 °C for 3 h under constant stirring at a rate of 1000 rpm. The working pressure in the reactor ranged from 9.1 to 11.5 MPa, depending on the process conditions.

After completion of the process and cooling the reaction mixture to room temperature, the gaseous products of the reaction were quantitatively discharged from the autoclave by washing off with ethanol and the obtained mixture of liquid and solid products was separated by filtration. The solid residue was washed with ethanol until the filtrate became colorless.

Ethanol was removed from the product solution on a rotary evaporator and the residue was brought to constant weight under vacuum (1 mm Hg) at room temperature. The liquid product yield (wt %) was calculated as

$$a_1 = \frac{m_1}{m_{fs}} \times 100\%, \quad (1)$$

where m_1 is the liquid product weight (g) and m_{fs} is the weight of flax shives (g).

The solid residue yield was calculated

$$asa_2 = \frac{m_{sr} - m_{cat}}{m_{fs}} \times 100\% \quad (2)$$

where m_{sr} is the solid residue weight (g) after the extraction and m_{cat} is the catalyst weight (g).

The flax shives conversion was determined using the formula

$$X_{fs} = \frac{m_{fs} - m_{sr} - m_{cat}}{m_{fs}} \times 100\% \quad (3)$$

The degree of delignification was calculated as

$$X_l = \frac{m_{fs} - m_{lsr}}{m_{lfs}} \times 100\% \quad (4)$$

where m_{lfs} and m_{lsr} is the weight of lignin in flax shives and in the solid residue (g), respectively.

The cellulose yield (wt %) was determined as

$$X_c = \frac{m_{csr}}{m_{cfs}} \times 100\% \quad (5)$$

where m_{cfs} and m_{csr} are the cellulose weights in flax shives and in the solid residue, respectively.

3.6. Analysis of the Hydrogenation Products of Flax Shives

The solid product of the thermal transformation of flax shives was analyzed for the contents of hemicelluloses, cellulose, and lignin. The residual lignin content in the solid product was determined by hydrolysis in 72% sulfuric acid using the Komarov method [47] and the hemicellulose content, by gas chromatography (GC) of the obtained hydrolysates. The content and composition of monosaccharides in the hydrolysates were found by GC using a VARIAN-450 GC gas chromatograph (Palo Alto, CA, USA) with a flame ionization detector and a VF-624ms capillary column with a length of 30 m and an inner diameter of 0.32 mm. The chromatography conditions were helium as a carrier gas, an injector temperature of 250 °C, an initial column temperature of 50 °C (5 min), a temperature increase to 180 °C at a rate of 10 °C/min, and holding at 180 °C for 37 min. Before the analysis, the hydrolyzate was derivatized using the technique from [48] to obtain trimethylsilyl derivatives. Sorbitol was used as an internal standard. Peaks were identified by times of retention of the tautomeric forms of monosaccharides. Cellulose was determined in the solid products of hydrogenation of flax shives using the nitrogen-alcohol (Kürschner–Hoffer) method [49,50].

The liquid ethanol-soluble products of hydrogenation of flax shives were subjected to GC-mass spectrometry (MS) analysis on an Agilent 7890A chromatograph with an HP-5MS capillary column (30 m) at temperature programming in the range of 40–250 °C and an Agilent 7000A Triple Quad selective mass spectrometer. The compounds were identified using the NIST MS Search 2.0 instrument database.

4. Conclusions

The reductive fractionation of flax shives over a nickel catalyst deposited on a Sibunit carbon support was studied. A comparison of the electronic states of nickel in the catalysts and product yields showed that the metal nickel of the catalyst determines, to a great extent, the formation of both 4-propyl guaiacol and monomers in general. It was shown that the catalyst studied increases the yield of monomeric products of lignin hydrogenation from 1.1 to 9.6% of lignin. The latter is less than the yield from the ruthenium catalyst by 30%, and this is probably due to the fact that two parallel destruction and condensation reactions occur in this process, and on a nickel catalyst it is impossible to accelerate the destruction as effectively to suppress the condensation reaction as on a ruthenium catalyst.

The effect of acid and alkaline pretreatment of shives on the product yields of their subsequent reductive catalytic fractionation was examined. It was shown that alkaline treatment enhances the cellulose yield in the process under study.

An increase in the stirring rate and a decrease in the catalyst grain size leads to several changes in the process: (a) they increase the degree of delignification and, consequently, reduce the lignin content in the solid residue; (b) they reduce the content of hemicelluloses in the solid residue; (c) they also cause a monotonic increase in the yield of monomeric compounds from 1.5 to 9.7 wt %. It was demonstrated that the process occurs mainly on the catalyst grain's outer surface, i.e., under the condition of external diffusion limitation.

The dependence of the cellulose yield on the mass transfer conditions are more complex; the catalyst drives two cellulose conversion processes, it stabilizes cellulose at large (0.1–2 mm) grain sizes and degrades it at the minimum grain size, i.e., at the maximum activity of the catalyst. A decrease in the stirring rate by a factor of 2–8 on the most active catalyst increases the cellulose yield by a factor of two or more, up to 92%, i.e., almost to its initial content in the shives. As a result, the best compromise on the cellulose yield and degree of delignification (85 and 86%, respectively) is obtained at the minimum grain size (54–96 µm) and average stirring rate (500 min⁻¹).

It was shown that the yield of liquid products in the catalytic process is increased by intensifying the mass transfer rate (from 14.6 to 24.6 wt %), but this yield is not attained in the non-catalytic process (38.5 wt %). The simplest explanation for this fact is that, on the catalyst surface, the processes of removal of the final and intermediate products into the bulk of the liquid phase compete with the catalytic condensation of soluble substances into the products determined as solids.

The influence of the mass transfer intensity on the composition of monomeric products supports the earlier suggested scheme for the formation of the products over bifunctional nickel catalysts. The obtained results demonstrate the possibility to change the content of the monomeric products by varying the mass transfer intensity.

Author Contributions: Conceptualization, V.E.T., Y.K. and O.P.T.; methodology, A.V.M., A.S.K., A.M.S. and V.E.T.; formal analysis, Y.L.M., A.I.C., V.V.S. and Y.K.; investigation, A.V.M., A.S.K., V.V.S., A.M.S., A.I.C. and Y.L.M.; data curation A.S.K., A.V.M., V.V.S., Y.L.M. and V.E.T.; writing—original draft preparation, A.V.M. and A.S.K.; writing—review and editing, V.E.T.; visualization, A.V.M. and V.V.S.; supervision, O.P.T. and V.E.T.; project administration, V.E.T.; funding acquisition, V.E.T. All authors have read and agreed to the published version of the manuscript.

Funding: This study was supported by the Russian Science Foundation, project no. 20-63-47109.

Data Availability Statement: Data available on request from the authors.

Acknowledgments: The experiments were conducted on the equipment of the Krasnoyarsk Regional Center for Collective Use, Krasnoyarsk Science Center of the Siberian Branch of the Russian Academy of Sciences.

Conflicts of Interest: The authors declare no conflict of interest.

References

1. Ross, K.; Giuseppe, M. Characteristics of Lignin from Flax Shives as Affected by Extraction Conditions. *Int. J. Mol. Sci.* **2010**, *11*, 4035–4050. [[CrossRef](#)]
2. Brosse, N.; Dufour, A.; Meng, X.; Sun, Q.; Ragauskas, A. Miscanthus: A fast-growing crop for biofuels and chemicals production. *Biofuels Bioprod. Biorefining* **2012**, *6*, 580–598. [[CrossRef](#)]
3. Wang, S.; Gao, W.; Li, H.; Xiao, L.-P.; Sun, R.-C.; Song, G. Selective Fragmentation of Biorefinery Corn cob Lignin into p-Hydroxycinnamic Esters with a Supported Zinc Molybdate Catalyst. *ChemSusChem* **2018**, *11*, 2114–2123. [[CrossRef](#)] [[PubMed](#)]
4. Lugovoy, Y.V.; Chalov, K.V.; Tarabanko, V.E.; Stepacheva, A.A.; Kosivtsov, Y.Y. Fast Pyrolysis of Flax Shive in a Screw-Type Reactor. *Chem. Eng. Technol.* **2021**, *44*, 2056–2063. [[CrossRef](#)]
5. Kim, S.; Dale, B.E. Global potential bioethanol production from wasted crops and crop residues. *Biomass Bioenergy* **2004**, *26*, 361–375. [[CrossRef](#)]
6. del Río, J.C.; Rencoret, J.; Gutiérrez, A.; Nieto, L.; Jiménez-Barbero, J.; Martínez, Á.T. Structural Characterization of Guaiacyl-rich Lignins in Flax (*Linum usitatissimum*) Fibers and Shives. *J. Agric. Food Chem.* **2011**, *59*, 11088–11099. [[CrossRef](#)] [[PubMed](#)]
7. Kuznetsov, B.N.; Sudakova, I.G.; Garyntseva, N.V.; Kondrasenko, A.A.; Pestunov, A.V.; Djakovitch, L.; Pinel, C. Catalytic peroxide fractionation processes for the green biorefinery of wood. *React. Kinet. Mech. Catal.* **2019**, *126*, 717–735. [[CrossRef](#)]
8. Tarabanko, V.E.; Kaygorodov, K.L.; Skiba, E.A.; Tarabanko, N.E.; Chelbina, Y.V.; Baybakova, O.V.; Kuznetsov, B.N.; Djakovitch, L. Processing Pine Wood into Vanillin and Glucose by Sequential Catalytic Oxidation and Enzymatic Hydrolysis. *Wood Chem. Technol.* **2017**, *37*, 43–51. [[CrossRef](#)]
9. Van den Bosch, S.; Schutyser, W.; Vanholme, R.; Driessen, T.; Koelewijn, S.F.; Renders, T.; De Meester, B.; Huijgen, W.J.J.; Dehaen, W.; Courtin, C.M.; et al. Reductive lignocellulose fractionation into soluble lignin-derived phenolic monomers and dimers and processable carbohydrate pulps. *Energy Environ. Sci.* **2015**, *8*, 1748–1763. [[CrossRef](#)]
10. Baryshnikov, S.V.; Miroshnikova, A.V.; Kazachenko, A.S.; Malyar, Y.N.; Taran, O.P.; Lavrenov, A.V.; Djakovitch, L.; Kuznetsov, B.N. Hydrogenation of abies wood and ethanol lignin by hydrogen in supercritical ethanol in the presence of bifunctional catalyst Pt/ZrO₂. *J. Sib. Fed. Univ. Chem.* **2019**, *12*, 550–561. [[CrossRef](#)]
11. Kuznetsov, B.N.; Chesnokov, N.V.; Sudakova, I.G.; Garyntseva, N.V.; Kuznetsova, S.A.; Malyar, Y.N.; Yakovlev, V.A.; Djakovitch, L. Green catalytic processing of native and organosolv lignins. *Catal. Today* **2018**, *309*, 18–30. [[CrossRef](#)]
12. Kazachenko, A.S.; Miroshnikova, A.V.; Tarabanko, V.E.; Skripnikov, A.M.; Malyar, Y.N.; Borovkova, V.S.; Sychev, V.V.; Taran, O.P. Thermal Conversion of Flax Shives in Sub- and Supercritical Ethanol in the Presence of Ru/C Catalyst. *Catalysts* **2021**, *11*, 970. [[CrossRef](#)]
13. Schutyser, W.; Van den Bosch, S.; Renders, T.; De Boe, T.; Koelewijn, S.F.; Dewaele, A.; Ennaert, T.; Verkinderen, O.; Goderis, B.; Courtin, C.M.; et al. Influence of bio-based solvents on the catalytic reductive fractionation of birch wood. *Green Chem.* **2015**, *17*, 5035–5045. [[CrossRef](#)]
14. Park, J.; Riaz, A.; Verma, D.; Lee, H.J.; Woo, H.M.; Kim, J. Fractionation of Lignocellulosic Biomass over Core–Shell Ni@Al₂O₃ Catalysts with Formic Acid as a Cocatalyst and Hydrogen Source. *ChemSusChem* **2019**, *12*, 1743–1762. [[CrossRef](#)]
15. Taran, O.P.; Sharypov, V.I.; Baryshnikov, S.V.; Beregovtsova, N.G.; Miroshnikova, A.V.; Kazachenko, A.S.; Sychev, V.V.; Kuznetsov, B.N. Reductive fractionation of larch in a supercritical ethanol medium in the presence of bifunctional Ru/C catalyst and hydrogen donor. *Katal. V Promyshlennosti* **2020**, *20*, 127–139. [[CrossRef](#)]
16. Renders, T.; Van den Bossche, G.; Vangeel, T.; Van Aelst, K.; Sels, B. Reductive catalytic fractionation: State of the art of the lignin-first biorefinery. *Curr. Opin. Biotechnol.* **2019**, *56*, 193–201. [[CrossRef](#)]
17. Schutyser, W.; Renders, T.; Van den Bosch, S.; Koelewijn, S.F.; Beckham, G.T.; Sels, B.F. Chemicals from lignin: An interplay of lignocellulose fractionation, depolymerisation, and upgrading. *Chem. Soc. Rev.* **2018**, *47*, 852–908. [[CrossRef](#)]
18. Li, C.; Zhao, X.; Wang, A.; Huber, G.W.; Zhang, T. Catalytic Transformation of Lignin for the Production of Chemicals and Fuels. *Chem. Rev.* **2015**, *115*, 11559–11624. [[CrossRef](#)]
19. Galkin, M.V.; Samec, J.S. Lignin Valorization through Catalytic Lignocellulose Fractionation: A Fundamental Platform for the Future Biorefinery. *ChemSusChem* **2016**, *9*, 1544–1558. [[CrossRef](#)]
20. Renders, T.; Van den Bosch, S.; Koelewijn, S.F.; Schutyser, W.; Sels, B.F. Lignin-first biomass fractionation: The advent of active stabilisation strategies. *Energy Environ. Sci.* **2017**, *10*, 1551–1557. [[CrossRef](#)]
21. Ayusheev, A.B.; Taran, O.P.; Afinogenova, I.I.; Mishchenko, T.I.; Shashkov, M.V.; Sashkina, K.A.; Semeikina, V.S.; Parkhomchuk, E.V.; Agabekov, V.E.; Parmon, V.N. Depolymerization of Birch-Wood Organosolv Lignin Over Solid Catalysts in Supercritical Ethanol. *J. Sib. Fed. Univ. Chem.* **2016**, *3*, 353–370. [[CrossRef](#)]
22. Chikunov, A.S.; Shashkov, M.V.; Pestunov, A.V.; Kazachenko, A.S.; Mishchenko, T.I.; Taran, O.P. Hydrogenolysis of Birch Ethanol-Lignin in Supercritical Over Bifunctional Ru and Ni Catalysts Bifunctional Supported on Oxidized Carbon. *J. Sib. Fed. Univ. Chem.* **2018**, *1*, 131–150. [[CrossRef](#)]

23. Michel, C.; Gallezot, P. Why Is Ruthenium an Efficient Catalyst for the Aqueous-Phase Hydrogenation of Biosourced Carbonyl Compounds? *ACS Catal.* **2015**, *5*, 4130–4132. [[CrossRef](#)]
24. Song, Q.; Wang, F.; Cai, J.; Wang, Y.; Zhang, J.; Yu, W.; Xu, J. Lignin depolymerization (LDP) in alcohol over nickel-based catalysts via a fragmentation–hydrogenolysis process. *Energy Environ. Sci.* **2013**, *6*, 994–1007. [[CrossRef](#)]
25. Anderson, E.M.; Katahira, R.; Reed, M.; Resch, M.G.; Karp, E.M.; Beckham, G.T.; Román-Leshkov, Y. Reductive Catalytic Fractionation of Corn Stover Lignin. *ACS Sustain. Chem. Eng.* **2016**, *4*, 6940–6950. [[CrossRef](#)]
26. Klein, I.; Saha, B.; Abu-Omar, M.M. Lignin depolymerization over Ni/C catalyst in methanol, a continuation: Effect of substrate and catalyst loading. *Catal. Sci. Technol.* **2015**, *5*, 3242–3245. [[CrossRef](#)]
27. Kuznetsov, B.N.; Baryshnikov, S.V.; Miroshnikova, A.V.; Kazachenko, A.S.; Malyar, Y.N.; Skripnikov, A.M.; Taran, O.P. Fractionation of Birch Wood by Integrating Alkaline-Acid Treatments and Hydrogenation in Ethanol over a Bifunctional Ruthenium Catalyst. *Catalysts* **2021**, *11*, 1362. [[CrossRef](#)]
28. Chen, Y.S.; Kang, J.F.; Chen, B.; Gao, B.; Liu, L.F.; Liu, X.Y.; Wang, Y.Y.; Wu, L.; Yu, H.Y.; Wang, J.Y.; et al. Microscopic mechanism for unipolar resistive switching behaviour of nickel oxides. *J. Phys. D Appl. Phys.* **2012**, *45*, 065303. [[CrossRef](#)]
29. Khandaker, S.; Kuba, T.; Toyohara, Y.; Kamida, S.; Uchikawa, Y. Development of ion-exchange properties of bamboo charcoal modified with concentrated nitric acid. *IOP Conf. Ser. Earth Environ. Sci.* **2017**, *82*, 012002. [[CrossRef](#)]
30. Kazachenko, A.S.; Tarabanko, V.E.; Miroshnikova, A.V.; Sychev, V.V.; Skripnikov, A.M.; Malyar, Y.N.; Mikhlin, Y.L.; Baryshnikov, S.V.; Taran, O.P. Reductive Catalytic Fractionation of Flax Shive over Ru/C Catalysts. *Catalysts* **2021**, *11*, 42. [[CrossRef](#)]
31. Tarabanko, V.E. Catalytic Conversion of Lignins for Valuable Chemicals. *Catalysts* **2021**, *11*, 1254. [[CrossRef](#)]
32. Chen, J.; Lu, F.; Si, X.; Nie, X.; Lu, R.; Xu, J. High Yield Production of Natural Phenolic Alcohols from Woody Biomass Using a Nickel-Based Catalyst. *ChemSusChem* **2016**, *9*, 3353–3360. [[CrossRef](#)] [[PubMed](#)]
33. Tarabanko, V.E.; Kaygorodov, K.L.; Vigul, D.O.; Tarabanko, N.; Chelbina, Y.V.; Smirnova, M.A. Influence of acid prehydrolysis on the process of wood oxidation into vanillin and pulp. *J. Wood Chem. Technol.* **2020**, *40*, 421–433. [[CrossRef](#)]
34. Xu, G.; Luo, Y.; Song, T.; He, B.; Chang, M.; Ren, J. Preparation and application of a xylan-based antibacterial papermaking additive to protect against *Escherichia coli* bacteria. *BioResources* **2020**, *15*, 4781–4801. [[CrossRef](#)]
35. Naidu, D.S.; Hlangothi, S.P.; John, M.J. Bio-based products from xylan: A review. *Carbohydr. Polym.* **2018**, *179*, 28–41. [[CrossRef](#)] [[PubMed](#)]
36. Du, X.; Pérez-Boada, M.; Fernández, C.; Rencoret, J.; del Río, J.C.; Jiménez-Barbero, J.; Li, J.; Gutiérrez, A.; Martínez, A.T. Analysis of lignin–carbohydrate and lignin–lignin linkages after hydrolase treatment of xylan–lignin, glucomannan–lignin and glucan–lignin complexes from spruce wood. *Planta* **2014**, *239*, 1079–1090. [[CrossRef](#)] [[PubMed](#)]
37. Zhao, Y.; Shakeel, U.; Rehman, M.S.U.; Li, H.; Xu, X.; Xu, J. Lignin-carbohydrate complexes (LCCs) and its role in biorefinery. *J. Clean. Prod.* **2020**, *253*, 120076. [[CrossRef](#)]
38. Sun, S.; Sun, S.; Cao, X.; Sun, R. The role of pretreatment in improving the enzymatic hydrolysis of lignocellulosic materials. *Bioresour. Technol.* **2016**, *199*, 49–58. [[CrossRef](#)]
39. Cao, S.; Pu, Y.; Studer, M.; Wyman, C.; Ragauskas, A.J. Chemical transformations of *Populus trichocarpa* during dilute acid pretreatment. *RSC Adv.* **2012**, *2*, 10925–10936. [[CrossRef](#)]
40. Bali, G.; Meng, X.; Deneff, J.I.; Sun, Q.; Ragauskas, A.J. The Effect of Alkaline Pretreatment Methods on Cellulose Structure and Accessibility. *ChemSusChem* **2015**, *8*, 275–279. [[CrossRef](#)]
41. Van den Bosch, S.; Renders, T.; Kennis, S.; Koelewijn, S.F.; Van den Bossche, G.; Vangeel, T.; Deneyer, A.; Depuydt, D.; Courtin, C.M.; Thevelein, J.M.; et al. Integrating lignin valorization and bio-ethanol production: On the role of Ni-Al₂O₃ catalyst pellets during lignin-first fractionation. *Green Chem.* **2017**, *19*, 3313–3326. [[CrossRef](#)]
42. Liu, X.; Li, H.; Xiao, L.-P.; Sun, R.-C.; Song, G. Chemodivergent hydrogenolysis of eucalyptus lignin with Ni@ZIF-8 catalyst. *Green Chem.* **2019**, *21*, 1498–1504. [[CrossRef](#)]
43. Taran, O.P.; Descorme, C.; Polyanskaya, E.M.; Ayusheev, A.B.; Besson, M.; Parmon, V.N. Sibunit-based catalytic materials for the deep oxidation of organic ecotoxicants in aqueous solutions. III: Wet air oxidation of phenol over oxidized carbon and Ru/C catalysts. *Catal. Ind.* **2013**, *5*, 164–174. [[CrossRef](#)]
44. Śrębowata, A.; Juszczak, W.; Kaszkar, Z.; Sobczak, J.W.; Kepiński, L.; Karpiński, Z. Hydrodechlorination of 1,2-dichloroethane and dichlorodifluoromethane over Ni/C catalysts: The effect of catalyst carbiding. *Appl. Catal. A Gen.* **2007**, *319*, 181–192. [[CrossRef](#)]
45. Tewari, P.H.; Campbell, A.B. Temperature dependence of point of zero charge of cobalt and nickel oxides and hydroxides. *J. Colloid Interface Sci.* **1976**, *55*, 531–539. [[CrossRef](#)]
46. Tarabanko, V.E.; Vigul, D.O.; Kaygorodov, K.L.; Kosivtsov, Y.; Tarabanko, N.; Chelbina, Y.V. Influence of mass transfer and acid prehydrolysis on the process of flax shives catalytic oxidation into vanillin and pulp. *Biomass Convers. Biorefinery* **2022**. [[CrossRef](#)]
47. Sluiter, J.B.; Ruiz, R.O.; Scarlata, C.J.; Sluiter, A.D.; Templeton, D.W. Compositional Analysis of Lignocellulosic Feedstocks. 1. Review and Description of Methods. *J. Agric. Food Chem.* **2010**, *58*, 9043–9053. [[CrossRef](#)]
48. Ruiz-Matute, A.I.; Hernández-Hernández, O.; Rodríguez-Sánchez, S.; Sanz, M.L.; Martínez-Castro, I. Derivatization of carbohydrates for GC and GC–MS analyses. *J. Chromatogr. B* **2011**, *879*, 1226–1240. [[CrossRef](#)]
49. Kürschner, K.; Hoffer, A. Ein neues Verfahren zur Bestimmung der Cellulose in Hölzern und Zellstoffen A new method for the determination of cellulose in wood and pulps. *Technol. Chem. Papier. Zellstoff. Fabr.* **1929**, *26*, 125–129.
50. Obolenskaya, A.V.; Elnitskaya, Z.P.; Leonovich, A.A. Laboratory Works on Chemistry of Wood and Cellulose. *Ecology* **1991**, *7*, 78–155.